Avestia Publishing
Journal Name: Journal of Fluid Flow, Heat and Mass Transfer (JFFHMT)
Volume 12, Year 2025
ISSN: 2368-6111
DOI: 10.11159/jffhmt.2025.006

Comparative Numerical study of the Thermal and Electrical Performance of Combined and Separated Solar Chimneys for Passive Space Cooling in Multi-Storey Buildings

Doubik Yemboate LARE [1], Yawovi NOUGBLEGA[1,2*], Kokou Dowou [1], Kokou Aménuvéla TOKA[1]
[1] Laboratoire Sur l'Energie Solaire /Groupe Phénomène de Transfert et Energétique,
Université de Lomé, 01 Lomé 01 BP 1515, Togo.
[2] Regional Centre of Excellence on Electricity Management (CERME),
University of Lomé, Togo.
*Corresponding author: ynougblega@univ-lome.tg

Abstract - *The present study employs numerical analysis to examine the thermal and electrical performance of distinct photovoltaic/thermal (PV/T) hybrid solar chimney configurations integrated into multi-story buildings, to enhance passive space cooling. Various configurations are considered, including a single chimney, a combined chimney, a separated chimney, and a shunt chimney. The focus is on the impact of multiple air inlets on circulation and heat dissipation. The modeling is based on a two-dimensional mixed convection model, utilizing the Boussinesq approximation to simulate heat exchange and air movement. The transfer equations are discretized using the finite difference technique. The resulting system of equations is then solved using the Thomas algorithm in combination with the iterative Gauss-Seidel method. Numerical simulations compared the performance of each configuration, focusing on heat transfer and electrical efficiency stability at different Reynolds numbers. The results show that the combined, separated, and shunt configurations significantly improve heat dissipation and electrical efficiency stability. In particular, the separated stack provides a homogeneous distribution of heat thanks to the segmentation of the airflow, which avoids hot spots and ensures more efficient cooling of the photovoltaic cells. These integrated PV/T systems, therefore, offer the potential to optimize the use of solar energy in multi-story buildings, while reducing energy requirements for passive cooling of interior spaces.*

Keywords: *Hybrid solar chimney, Passive cooling, Mixed convection, Thermal dissipation, Electrical efficiency*

1. Introduction

In a combined photovoltaic/thermal (PV/T) solar system, two modules are employed: one photovoltaic and the other for the collection of thermal energy. The system can transform solar energy into both electrical and thermal energy[1]. Research into PV/T energy systems has attracted significant attention in the solar energy field in recent years, as they offer a means of enhancing the efficiency of solar energy utilization. In recent decades, researchers have dedicated their attention to the development of photovoltaic-thermal (PV/T) technology. In addition to the aforementioned literature, several original systems and products have been proposed by the authors [1]. PV/T collectors can be classified into two categories, depending on the means of cooling employed: liquid-based and air-based. Liquid-based PV/T collectors employ a liquid medium, such as water, in conjunction with a nanofluid for cooling purposes.

In a study conducted by Nualboonrueng et al. [2], the performance of water-based photovoltaic/thermal (PV/T) collectors was assessed under real-world

Date Received: 2024-11-22
Date Revised: 2024-12-12
Date Accepted: 2025-01-29
Date Published: 2025-02-21

climatic conditions in Bangkok. The objective was to confirm the electrical and thermal energy provided by the collector in tropical areas. Jahromi et al. [3] performed an energy and economic evaluation of a PV/T water collector employing a MATLAB simulation. Rosa-Clot et al.[4]conducted an experimental assessment of the thermal and electrical performance of the PV/T water collector, additionally comparing its electrical efficiency with that of a PV system. Mohammed El Hadi Attia et al[5] presented an improved design of PV-T systems incorporating finned cooling channels and a two-phase nano-fluid air/TiO2-water. Simulations show a significant increase in thermal and electrical efficiency, offering promising potential for building applications.

The use of a liquid as a cooling medium results in relatively high thermal efficiency due to the high thermal conductivity of liquids. However, due to the intricate nature of their design, liquid-based PV/T collectors are costly to produce and are susceptible to freezing during operation in winter. Conversely, air PV/T collectors are cost-effective due to their simple design and minimal maintenance requirements. Nevertheless, the heat transfer performance of PV/T air collectors is inadequate due to the low thermal conductivity of air. Over the past decade, numerous attempts have been made to enhance the functionality of the PV/T air system, with the incorporation of diverse design and modification elements. For instance, Slimenai et al. [6]conducted a comparative numerical study comparing PV modules with three distinct types of PV/T air collectors in the context of Algiers climatic conditions. The results indicated that the glazed double-pass collector exhibited the most favorable overall daily energy efficiency, achieving an average of 74%. Malagouda Patil et al.[7] analyzed the impact of an air cooling system on the operating temperature and performance of photovoltaic (PV) panels. The experimental installation, attached to the back of the panels, reduced their average temperature by 9°C, with maximum measured temperatures of 45.60°C (with cooling) compared with 50.24°C (without cooling), for an optimum air flow rate of 0.08 kg/s. This thermal reduction resulted in a significant increase in the energy conversion efficiency of the panels, from 7% to 12.6%. The results show that air cooling is an effective solution for preventing overheating of the panels and improving their overall efficiency. [8]put forward a novel design comprising two low-cost alterations to the conventional PV/T hybrid air collector system. To create a PV/T air system, a thin, flat sheet is suspended in the center of the air duct, or an extended surface is created on the walls of the air duct. The results indicated that the modifications are highly effective in extracting thermal energy and maintaining lower temperatures for the photovoltaic (PV) modules, thereby enhancing overall system efficiency. The impact of duct depth, channel length, and airflow rate on the overall performance of the PV/T hybrid air system was investigated through the application of validated numerical techniques. Experimental work was conducted in Busan, South Korea, on a novel photovoltaic/thermal (PV/T) single-pass dual-flow air channel collector, featuring a non-uniform cross-sectional rib, attached to the back of a photovoltaic (PV) module by Choi et al. [9]. The maximum electricity efficiency and overall thermal efficiency were 14.81% and 71.54%, respectively, for a mass flow rate of 0.07698 kg/s. Badi et al [10] put forth a passive cooling system for photovoltaic panels comprising an inclined channel with adiabatic extensions for the removal of heat through natural convection. This method enhances airflow by 65% and mitigates the maximum temperature by 11%, thus optimizing the yield and lifespan of photovoltaic panels in climates characterized by elevated temperatures.

In an examination of the thermal performance of a PV-T air collector, Naima Boulfaf [11] conducted theoretical and numerical studies in dynamic mode to analyze the collector's behaviour. A thermal model was developed employing the finite element method, whereby temperature profiles for various components were established, including glazing, solar cells, and outlet air. The analysis revealed that the solar cells reached the highest temperatures, while the length of the collector and the air velocity exerted a considerable influence on the thermal efficiency of the system. An increase in airspeed, specifically from 0 to 1 m/s, serves to reduce the temperature of the photovoltaic (PV) module, particularly by cooling the solar cells. This study is concerned with the simulation and optimization of an innovative air-cooled photovoltaic/thermal (PV-T) collector, which employs thermal micro-pipes to enhance performance. Wan Yu et al. [12] developed a numerical model for the analysis of the thermal and electrical behaviour of the collector under different operating conditions. The incorporation of thermal micro-pipes facilitates enhanced heat dissipation, thereby reducing the temperature of the photovoltaic cells and improving electrical efficiency. The outcomes demonstrate that this system enhances overall efficiency relative to conventional PV-T collectors. Optimization of

the design parameters, including the configuration of the micro-pipes and the airflow, serves to enhance the performance of the system as a whole. In a separate study, S Zine et al. [13] conducted an experimental investigation into the thermal and electrical performance of an air-cooled photovoltaic/thermal (PV-T) hybrid solar collector for domestic use. The PV-T system makes use of air as a heat transfer medium to extract heat generated by photovoltaic cells. This has the effect of improving the efficiency of electricity production by reducing operating temperatures. The experiments employed a temperature monitoring system to assess the temperature of the cells and the air leaving the collector, in addition to quantifying the heat flow transferred between the different layers of the collector. The transfer of thermal energy is optimized with an increase in airflow rate, resulting in enhanced cooling of the photovoltaic cells. The results demonstrate that this cooling mechanism improves the electrical efficiency of the system while providing warm air that can be utilized for domestic applications such as heating. A comprehensive analysis of the overall thermal efficiency of the system was conducted, taking into account a range of operating parameters, including solar radiation intensity and air flow rate. The results demonstrate the effectiveness of the PV-T collector with air cooling in enhancing both electricity generation and heat utilization in a residential context. In a study conducted by Shahsavar and Ameri[14], a photovoltaic/thermal (PV/T) air collector was designed, comprising a thin aluminum foil suspended in the middle of the air channel. The thermal characteristics of this collector were then examined under both natural and forced convection conditions, with and without a glass cover. Nguyen Van Hap et al[15] explored the performance of photovoltaic-thermal (PV-T) systems incorporating air heating. They performed a parametric analysis to assess the effect of various factors, such as air flow rate, solar intensity, and channel design, on overall thermal and electrical efficiency. An optimization methodology was used to identify the ideal configurations for maximizing heat recovery while maintaining high electrical output. The results highlight the potential of air-cooled PV-T systems as versatile and efficient energy solutions for residential and industrial applications. Assoa and Menezo [16] conducted simulations of air-cooled PV/T collectors utilizing either natural or forced ventilation. Their findings indicated that the thermal efficiency of PV/T collectors employing forced ventilation was superior to that of PV/T collectors utilizing natural ventilation. Kamel Sahlaoui et al [17]evaluated the thermal and electrical performance of a hybrid photovoltaic-thermal (PV/T) collector using air as the cooling medium. A study combining numerical simulations and experiments examined the effect of parameters such as air flow rate, solar irradiation conditions and collector design. The results show that the PV/T air system improves thermal efficiency through better heat management, while increasing electrical efficiency by reducing panel temperature. These results confirm the potential of hybrid PV/T collectors to optimise energy production in sustainable applications. The integration of photovoltaic and thermal (BIPV/T) systems within building envelopes allows for the collection of solar energy, which can be harnessed to generate both electricity and useful heat. This approach offers a highly efficient method for reducing the costs and consumption of energy used within buildings. The BIPV/T concept originated in the 1990s [18], as evidenced by the installation of a BIPV/T system on a restaurant rooftop in North Carolina, USA. This demonstration system was implemented as part of a PV Bonus initiative, to produce electricity and hot water [18]. The research into water-based BIPV/T systems is primarily focused on regions experiencing high temperatures. Examples of such research include projects in Hefei and Hong Kong[19]. To provide passive space heating in the winter and water heating during milder weather, a dual-purpose BIPV/T collector is utilized that employs natural circulation. A finite-difference model was devised which takes into account the characteristics of the collector and the manner of its integration into the building[20]. Subsequently, the model was subjected to field experimentation to ascertain its validity. It was found that a natural water circulation system was more efficient than a forced water circulation system, in terms of the system's thermal performance. In the climatic conditions prevalent in Hong Kong, the annual thermal and electrical efficiencies attained were 37.5% and 9.39%, respectively. Moreover, it was demonstrated that the BIPV/T system reduced overall thermal transmittance to 38% of that exhibited by a conventional building wall. BIPV/T systems in the air, on the other hand, have been studied in both cold and hot regions. Chen et al [21] presented a two-story, low-energy, prefabricated, single-family solar house in Quebec, Canada, with an open-loop, air-based BIPV/T system thermally coupled to a ventilated concrete slab. It was found that a BIPV/T system can significantly reduce the temperature of the

photovoltaic panels and has great potential for space heating support. To avoid snow cover during the cold winter period, Nagano et al [22] developed an air-oriented BIPV/T system integrated with vertical exterior wall panels. For two full months, from December 1999 to January 2000, comparative outdoor experiments were conducted with different BIPV/T systems.The introduction of a supplementary glass covering in front of the photovoltaic modules resulted in a notable increase in thermal efficiency, from approximately 22% to 29%. However, this improvement was accompanied by a concurrent decrease in electrical efficiency, from around 11% to 9%. This reduction can be attributed to the formation of condensation on the inner glass surface, the elevated temperature of the photovoltaic cells, and the reduction in the transmission of solar radiation onto the PV surface. In a separate study, Pantic et al [23] investigated the possibility of enhancing the efficiency of the BIPV/T system by integrating a 1.5 m vertical glazed air collector in parallel with the BIPV/T system outlet. During the period of low solar altitude in December and January, the solar air collector received considerable solar irradiation, resulting in the generation of warm air suitable for coupling with rock heat storage. The investigation revealed that the incorporation of a small vertical solar air heater into the unglazed BIPV/T system led to an enhancement in thermal energy production during the period of low solar irradiation. Despite the improved thermal efficiency of an air-cooled PV/T system, the air channel outlet temperature is often higher, leading to overheating of the photovoltaic cells. Nonetheless, the proliferation of heat within the photovoltaic cells represents a considerable obstacle to the optimal functioning of these systems, as it diminishes their electrical efficiency. It has been established by previous research that effective heat management is of paramount importance for the sustained high efficiency of PV/T systems. To remedy this situation, novel solar chimney configurations, including combined, separated, and shunt chimneys, have been put forth in this study as a means of enhancing the dissipation and ventilation of PV modules. This research project employs a computational approach to investigate the thermal and electrical functionality of distinct solar chimney configurations integrated into multi-story edifices. Of particular interest are the effects of incorporating multiple air inlets, which may facilitate more effective airflow and heat dissipation, reducing the probability of overheating while enhancing system-level efficiency. The findings of this study may provide valuable insights for advancing the development of more effective passive cooling techniques and solar photovoltaic energy generation systems. These developments could prove beneficial for meeting the rising demand for renewable energy in the built environment.

This study aims to compare the electrical and thermal performance of a multi-inlet photovoltaic/thermoelectric (PV/T) air system with that of a single-inlet PV/T collector. The present study will employ numerical analysis to investigate a mixed convection problem in a vertical PV/T hybrid thermal energy storage system, which is equipped with multiple inlets and is subjected to a constant heat flux for heating and ventilation. In this study, the airflow is introduced into the structure via internal openings and subsequently exits through an external port.

2. **Mathematical formulation**

2.1 Physical model

The objective of this study is to assess the impact of air circulation on the three pioneering types of vertical solar chimneys that can be incorporated into a multi-story structure. They comprise a PV/T collector with a H-shaped configuration. The solar chimney features three distinct levels of fresh air intake. The second chimney comprises a shunt duct of width d_2 which allows the introduction of fresh air into the main duct of width d_1, thus enabling the removal of excess heat from the solar cells. The third chimney is equipped with three inlets and three outlets. A comparative analysis will be conducted to examine the thermal and electrical performance of the three chimney types under consideration and evaluate their relative efficacy in comparison to a traditional vertical chimney. To extract the surplus heat produced by the solar cells, air is utilized as the heat transfer medium in the main channel. A two-dimensional (2D) transient laminar mixed convection model has been postulated. The transfer equations were formulated on the assumption that the thermophysical properties of the air remain constant and that the fluid is incompressible. The Boussinesq approximation was employed.

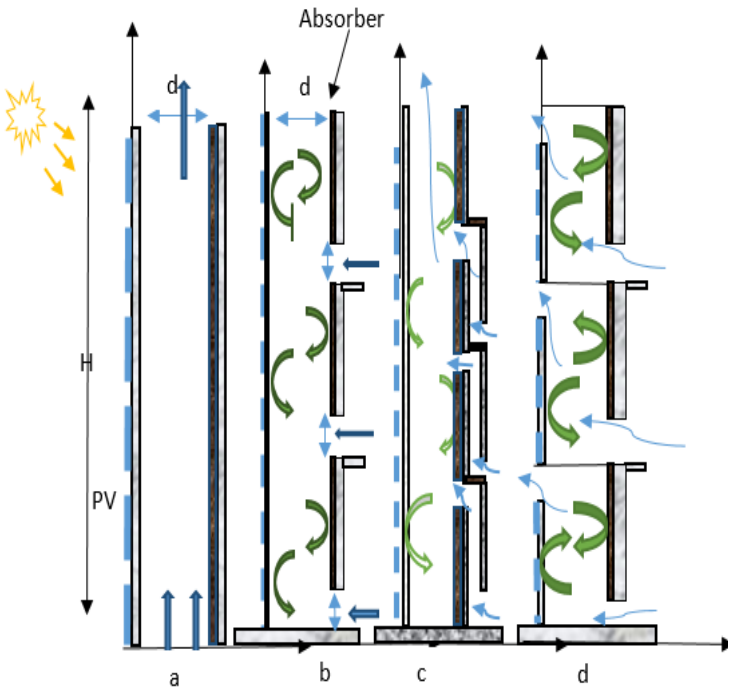

Figure 1 diagram of the physical model of solar chimneys: a) simple chimney b) combined chimney c) shunt chimney d) separated chimney

2.2 Governing equations

Continuity equation

$$\frac{\partial U}{\partial X}+\frac{\partial V}{\partial Y}=0 \tag{1}$$

Movement equation

$$\frac{\partial \Omega}{\partial \tau}+U\frac{\partial \Omega}{\partial X}+V\frac{\partial \Omega}{\partial Y} = \frac{1}{R_e}\left(\frac{\partial^2 \Omega}{\partial X^2}+\frac{\partial^2 \Omega}{\partial Y^2}\right) + R_i\frac{\partial \theta}{\partial X} \tag{2}$$

Energy equation

$$\frac{\partial \theta}{\partial \tau}+U\frac{\partial \theta}{\partial X}+V\frac{\partial \theta}{\partial Y}=\frac{1}{R_e P_r}\left(\frac{\partial^2 \theta}{\partial X^2}+\frac{\partial^2 \theta}{\partial Y^2}\right) \tag{3}$$

2.3 Associated boundary conditions

Initial conditions

At $\tau = 0,\ \theta = \Omega = \Psi = U = V = 0$

At $\tau > 0$

Combined chimney

$$X = 0; 0 < Y < D$$
$$U = V = 0; \Omega = -\left.\frac{\partial^2 \Psi}{\partial X^2}\right|_{X=0} \tag{4}$$
$$\left.\frac{\partial \theta}{\partial X}\right|_{X=0} = -(\tau_{gl}\alpha_{pv} - \eta_e)$$

$$X = 1; K < Y < D$$
$$U = V = 0; \Omega = -\left.\frac{\partial^2 \Psi}{\partial X^2}\right|_{X=1} \tag{5}$$
$$\left.\frac{\partial \theta}{\partial X}\right|_{X=1} = (\tau_{gl}\alpha_{abs}\alpha_{PV})$$

$$X = 1; 0 < Y < S$$
$$U = V = 0; \Omega = -\left.\frac{\partial^2 \Psi}{\partial X^2}\right|_{X=1} \tag{6}$$
$$\left.\frac{\partial \theta}{\partial X}\right|_{X=1} = (\tau_{gl}\alpha_{abs}\alpha_{PV})$$

$$X = 1; P < Y < A$$
$$U = V = 0; \Omega = -\left.\frac{\partial^2 \Psi}{\partial X^2}\right|_{X=1} \tag{7}$$
$$\left.\frac{\partial \theta}{\partial X}\right|_{X=1} = (\tau_{gl}\alpha_{abs}\alpha_{PV})$$

$$X = 1; A < Y < K$$
$$U = -1; V = 0; \Psi = -Y; \Omega = -\left.\frac{\partial^2 \Psi}{\partial X^2}\right|_{X=1}$$
$$\theta = 0 \tag{8}$$
$$X = 1; 0 < Y < T$$
$$U = -1; V = 0; \Psi = -Y; \Omega = -\left.\frac{\partial^2 \Psi}{\partial X^2}\right|_{X=1}$$

$$\theta = 0$$
$$X = 1; S < Y < P \tag{9}$$
$$U = -1; V = 0; \Psi = -Y$$

$$\Omega = -\left.\frac{\partial^2 \Psi}{\partial X^2}\right|_{X=1}; \theta = 0 \tag{10}$$

$$Y = D; 0 < X < 1$$

$$\left.\frac{\partial U}{\partial Y}\right|_{Y=D} = 0; \left.\frac{\partial V}{\partial Y}\right|_{Y=D} = 0$$
$$\left.\frac{\partial^2 \Psi}{\partial Y^2}\right|_{Y=D} = 0; \left.\frac{\partial \theta}{\partial Y}\right|_{Y=D} = 0 \quad (11)$$

Shunt chimney

$$X = 0; 0 < Y < D$$
$$U = V = 0; \Omega = -\left.\frac{\partial^2 \Psi}{\partial X^2}\right|_{X=0} \quad (12)$$
$$\left.\frac{\partial \theta}{\partial X}\right|_{X=0} = -\left(\tau_{gl}\alpha_{pv} - \eta_e\right)$$

$$Y = 0; 0 < X < 1$$
$$U = V = 0; \Omega = -\left.\frac{\partial^2 \Psi}{\partial Y^2}\right|_{Y=0}; \left.\frac{\partial^2 \Psi}{\partial Y^2}\right|_{Y=0} = 0 \quad (13)$$
$$\left.\frac{\partial \theta}{\partial Y}\right|_{Y=0} = 0$$

Absorber plates

$$X = B$$
$$U = V = 0; \Omega = -\left.\frac{\partial^2 \Psi}{\partial X^2}\right|_{X=B}; \left.\frac{\partial \theta}{\partial X}\right|_{X=B} = \left(\tau_{gl}\alpha_{abs}\alpha_{PV}\right) \quad (14)$$

Inlet openings

$$X = 1$$
$$U = -1; V = 0; \Psi = -Y; \Omega = -\left.\frac{\partial^2 \Psi}{\partial X^2}\right|_{X=1}; \theta = 0 \quad (15)$$

$$U = \frac{\partial \Psi}{\partial X}; V = -\frac{\partial \Psi}{\partial Y}; \Omega = -\left(\frac{\partial^2 \Psi}{\partial X^2} + \frac{\partial^2 \Psi}{\partial Y^2}\right) \quad (16)$$

Simple chimney

$$X = 0; 0 < Y < D$$
$$U = V = 0; \Omega = -\left.\frac{\partial^2 \Psi}{\partial X^2}\right|_{X=0} \quad (17)$$
$$\left.\frac{\partial \theta}{\partial X}\right|_{X=0} = -\left(\tau_{gl}\alpha_{pv} - \eta_e\right)$$

$$X = 1; 0 < Y < D$$
$$U = V = 0; \Omega = -\left.\frac{\partial^2 \Psi}{\partial X^2}\right|_{X=1} \quad (18)$$
$$\left.\frac{\partial \theta}{\partial X}\right|_{X=1} = \left(\tau_{gl}\alpha_{abs}\alpha_{PV}\right)$$

$$Y = 0; 0 < X < 1$$
$$U = 0; V = 1; \Psi = -X; \Omega = -\left.\frac{\partial^2 \Psi}{\partial X^2}\right|_{X=1}; \theta = 0 \quad (19)$$

$$Y = 0; 0 < X < 1$$
$$U = V = 0; \Omega = -\left.\frac{\partial^2 \Psi}{\partial Y^2}\right|_{Y=0}; \left.\frac{\partial^2 \Psi}{\partial Y^2}\right|_{Y=0} = 0; \left.\frac{\partial \theta}{\partial Y}\right|_{Y=0} = 0 \quad (20)$$

Separated chimney

At the inlets

$$X = 1$$
$$U = -1; V = 0\ ;\ \Psi = -Y; \Omega = -\left.\frac{\partial^2 \Psi}{\partial X^2}\right|_{X=1}; \theta = 0 \quad (21)$$

On the PV level

$$X = 0$$
$$U = V = 0\ ;\ \Omega = -\left.\frac{\partial^2 \Psi}{\partial X^2}\right|_{X=0}; \left.\frac{\partial \theta}{\partial X}\right|_{X=0} = -\left(\tau_{gl}\alpha_{pv} - \eta_e\right) \quad (22)$$

Absorbers:

$$X = 1$$
$$U = V = 0\ ;\ \Omega = -\left.\frac{\partial^2 \Psi}{\partial X^2}\right|_{X=1}\ ; \left.\frac{\partial \theta}{\partial X}\right|_{X=1} = \left(\tau_{gl}\alpha_{abs}\alpha_{PV}\right) \quad (23)$$

2.4 Assessment of Heat Transfer Intensity

The transfer of heat through vertical walls subjected to heating may be described in terms of the

Nuselt number, which represents a ratio of the conductive transfer of heat to the convective flux through the refrigerant. The following formula may calculate the local Nusselt number on the active plate with the photovoltaic (PV) cells at the coordinate *X*=0.

$$N_{uPV} = 1/\theta(Y) \tag{24}$$

The electrical efficiency of a photovoltaic solar cells is expressed in the following way:

$$\boldsymbol{\eta_{el}} = \eta_{ref} + \beta_{PV}(\Theta_{PV} - 298) + \gamma\log(\frac{\varphi}{1000}) \tag{25}$$

The following relationship is used to evaluate the thermal efficiency of the chimney:

$$\eta_{th} = \frac{\dot{m}C_{air}(T_0 - T_i)}{S_0 Q_0} \tag{26}$$

$$\Theta_{PV} = \frac{1}{H}\int_0^H T_{PV}(y)dy \tag{27}$$

$$\dot{m} = \int_0^1 V(X, A)dx \tag{28}$$

formerΘ_{PV} is the average temperature of the PV, T_0 is the temperature of the air leaving the chimney and T_i is the temperature of the air entering the chimney.

2.5 Numerical procedure

The differential equations that govern the transfer of heat and mass in a solar chimney are solved using the finite difference method. To circumvent potential instabilities commonly observed in mixed convection problems, a second-order upwind method was implemented for the convective components, whereas the central difference methodology was adopted to approximate the first- and second-order derivatives of the diffusive terms. The algebraic equations (2) and (3) were integrated using the Thomas algorithm. At each iteration, the successive point sub-relaxation method was applied to the Poisson equation, Eq. (4). It was determined that the optimal sub-relaxation coefficient was 0.8 for the 51×101 grid previously utilized in this study. The solution obtained at each time step exhibits iteration convergence. To confirm the existence of a stable solution, a condition must be satisfied.

It is presumed that solutions will converge when the absolute value of the relative error for each variable between successive iterations is less than a predetermined value, denoted ϵ, such as $\sum\left|\frac{\varphi^t(i,j)-\varphi^{t-1}(i,j)}{\varphi^t(i,j)}\right| \leq 10^{-5}$. In the aforementioned equation, the variable φ is equal to ψ, Θ, and ω, while the parameter t represents the number of iterations. A time step of 10^{-5} was deemed appropriate for the calculations. The approximation of wall vorticity is achieved through the implementation of the Woods formula. $\omega_W = \frac{1}{2}\omega_{W+1} - \frac{3}{\Delta\delta^2}(\psi_W - \psi_{W+1})$. In this context, ψ_W and ψ_{W+1} represent the values of the stream function at points adjoining the boundary wall. While δ is oriented in a normal vector to the boundary wall.

2.6 Mesh grid refinement study

The objective is to reduce the mesh's influence on the simulation's accuracy. To achieve this, mesh-independent solutions are ensured by comparing different meshes, with the highest Rayleigh and Reynolds numbers used in the present work (Ra = 3.10^5 and Re = 150) taken into account. As illustrated in Table 1, minor deviations are observed in the characteristic quantities Ψ, Θ, and Nu for non-uniform 21x51 and 51x101 meshes, compared to their uniform counterparts, the 51x51 and 101x101 meshes. Adopting a heterogeneous mesh configuration allows for the optimization of resolution, thereby facilitating a superior geometric representation of the model. This approach also serves to reduce numerical errors and enhance computational efficiency. However, the 51x101 mesh was selected due to its enhanced efficiency in heat transfer in comparison to the 21x51 mesh, as indicated by a 2.48% augmentation in the Nusselt number. The data about the electrical and thermo-optical properties of the walls used in the computations are presented in Table 2.

Table 1: Mesh sensitivity study

Mesh	Ψmax	Change (%)	Θmax	Change (%)	Numax	Change (%)
21X51	-0.0220	~	0.036	~	58.65	~
51X101	-0.0227	3.18	0.039	4.34	60.07	2.42
51X51	-0.020	~	0.048	~	57.02	~
101X101	-0.01	50	0.058	20.83	65.45	14.75

Table 2: Electrical and thermo-optical properties of walls

Parameters	Value
Absorptivity of PV cells surface, α_{pv}	0.89 (-)
Transmittance of PV cells surface, τ_{pv}	0.09 (-)
The reference temperature, T_{ref}	293 K
Electrical efficiency at the reference temperature, η_{ref}	0.015(-)
Temperature coefficient of PV cell, β_{ref}	0.0045 K^{-1}

3. Results and Discussion

3.1 Cumputer code validation

The developed calculation code was tested by presenting the stationary laminar mixed convection problem in a ventilated square cavity. The aforementioned cavity is furnished with an air inlet and an air outlet and is filled with air (Pr = 0.71). One wall of the cavity is maintained at a constant temperature, Tc (the bottom wall), while the remaining walls are treated as adiabatic boundaries. The solution of the test problem exhibits a high degree of agreement with the solutions of the ventilated cavity, as reported by Bouabdallah et al. [24], for a Grashof number fixed at 10^5 and a Richardson number fixed at 20. The results are presented in Figure 2.

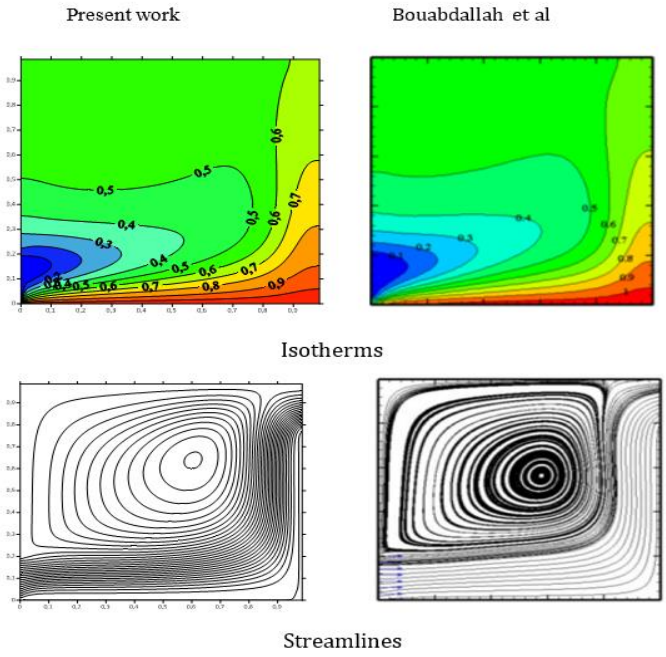

Figure 2: streamlines and isotherms for validation

3.2 Visualization of streamlines and isotherms in the chimneys

The structure of the streamlines and the temperature distribution are presented for an aspect ratio (B=H/d) equal to 8, to facilitate analysis of the aforementioned parameters. The streamlines and isotherms are depicted for steady-state flows obtained for a fixed Rayleigh number (Ra) = 10^5, with the Reynolds number fixed at 100. Figure 3 illustrates the direction and velocity of airflow within each stacked model, as indicated by the streamlines.

The simplest of the aforementioned stacks is represented by the diagram labeled 'a. The streamlines are predominantly vertical, indicating a steady ascent of air. The lack of divergence in the flow lines indicates the presence of an unidirectional and uniform airflow, with velocity dependent on the temperature differential. In the Combined stack (b), the streamlines are influenced by the presence of photovoltaic panels and a thermal absorber plate, which increase the air temperature and accelerate the airflow. The intensification of the circulation near the heat transfer surfaces is evident from the flow lines. Whereas a separated chimney is represented by symbol (c); the airflow is distributed across multiple sections, facilitating enhanced regulation of the ventilation process. This model incorporates a variation in flow between the different sections, facilitating the regulation of airflow velocity as required. Then, the fourth shunt is designated as Shunt Stack (d). As shown in the flow lines, the air is partially diverted, contingent on the desired ventilation conditions. The shunt enables the main flow to be diverted, which may be beneficial for regulating the pressure and temperature within the chimney. This model provides the flexibility required for the management of draughts. As illustrated in Figure 4, the temperature distributions within the different chimney types can be visualized using the isotherms presented therein. In the simple chimney (a), the isotherms display a high level of parallelism along the length of the chimney, indicating a gradual increase in air temperature by elevation. The rate of ascent of the airstream is directly proportional to the temperature difference between the base and the top of the chimney.

In the combined chimney configuration (b), the isotherms exhibit a more substantial increase in temperature, particularly in the vicinity of the heat absorber. The temperature variations are more pronounced, resulting in a higher thermal gradient and,

consequently, a more rapid airflow. In the separated chimney design(c), the isotherms are markedly discontinuous, indicative of disparate thermal zones. This can assist in distributing heat more equitably across the entire structure, thereby preventing the formation of concentrated hotspots. Such a method of distribution is likely to prove more effective in spaces where stable thermal regulation is required. The shunt chimney (d) is a type of chimney that diverts airflow in a different direction from the main flow. The isotherms are more dispersed, indicating that there is heat modulation occurring within the diverted airflow. The temperature dispersion evinced thereby evinces the aptitude of this model to modulate the thermal dispersion following the requisite specifications, thus enabling the indoor temperature to be regulated with greater precision.

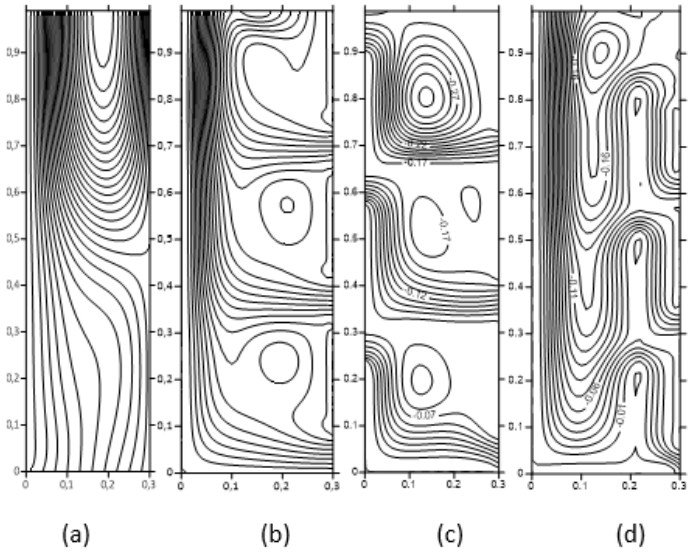

Figure3: Streamline visualization a) single chimney b) combined chimney c) separated chimney d) shunt chimney

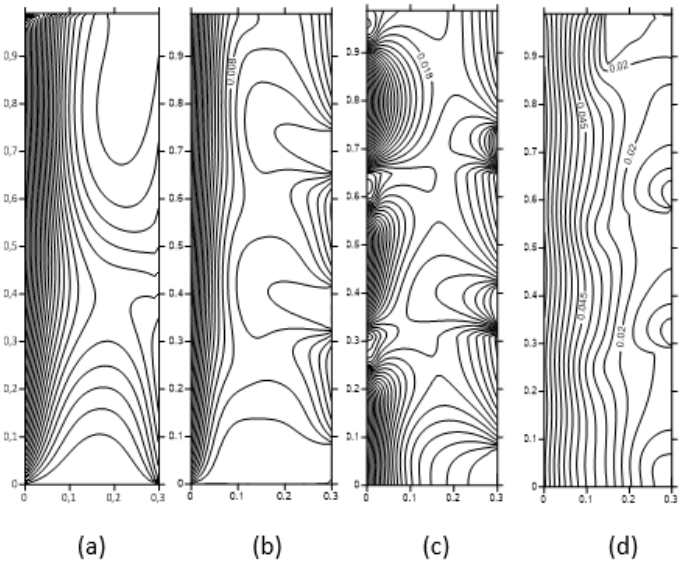

Figure 4: isotherms visualization a) single chimney b) combined chimney c) separated chimney d) shunt chimney

3.3 Influence of Reynolds number

3.3.1 Visualization of dynamic and thermal fields

For the aspect ratio (B=H/d) equalling 8, the structure of the streamline pattern and the temperature distribution are presented by varying the Reynolds number. **Figure 6** depicts the air dynamics and temperature distribution within the single stack at varying Reynolds numbers (Re = 50, 100, 150). At a Reynolds number of 50, the streamlines demonstrate a predominantly vertical upward airflow, which indicates a moderate degree of natural convection due to the temperature difference between the inlet and outlet of the stack. Upon reaching Reynolds numbers of 100 and 150, the flow density and air current speeds both increase, indicating an enhanced state of natural convection and air circulation within the stack. Nevertheless, the straightforward nature of this configuration restricts the potential for optimizing the flow for enhanced heat transfer. Then as the Reynolds number (Re) increases to 50, the isotherms demonstrate a greater spacing, indicative of a low-temperature gradient. At higher Reynolds numbers, the isotherms become more concentrated, indicative of elevated temperatures and augmented upward thermal transfer. This indicates the potential for greater cooling of photovoltaic cells through increased airflow, although the efficiency is still less than that of more complex configurations.

Figure 7 presents a visual representation of the combined stack configuration with multiple air inlets,

evaluated for identical Re values. In this configuration, the thermal absorber facilitates the advancement of the airflow by increasing the temperature of the surrounding air. At a Reynolds number of 50, an enhancement in the intensity of the air currents is observed in the vicinity of the absorber. At Reynolds numbers of 100 and 150, the intensification is even more pronounced, demonstrating enhanced air dynamics and improved heat dissipation from the photovoltaic panels. In the aforementioned configuration, the isotherms demonstrate the following characteristics. The isotherms illustrated in this configuration demonstrate a comparatively rapid elevation in temperature near the absorbers. The concentration of heat in the aforementioned area generates a higher thermal gradient in comparison with that of a simple chimney. This configuration thus exhibits enhanced thermal efficiency, with the potential for more efficient cooling of the photovoltaic panels due to a more dynamic airflow. **Figure 8** examines the effect of the separated chimney on the internal airflow. The chimney in question exhibits a distinct segmentation effect upon the flow of air. The streamlines of the separated stack demonstrate how the air flows through the segments at varying Reynolds numbers (i.e., 50, 100, 150). At Reynolds number 50, there is a moderate rate of airflow and a relatively uniform upward movement of air. An increase in the Reynold number (Re) to 100 results in the flow becoming significantly denser, thereby enhancing both circulation and heat transfer. At Reynolds number 150, the air velocity is considerably higher, thereby enabling rapid heat removal. The segmentation of the chimney ensures an even distribution of fresh air, thereby optimizing cooling at each level. The isotherms demonstrate the temperature distribution across the individual stacks for varying values of the Reynolds number (Re) parameter. At Re equal to 50, the temperature gradients are relatively insignificant; however, the segmentation has the effect of limiting the extent of the hot zones. At Re=100, the isotherms exhibit a greater degree of proximity to the walls, thereby suggesting enhanced efficiency in the transfer of heat. At Re=150, the thermal gradient is markedly more pronounced, with enhanced heat absorption by the air. The segmentation of the chimney ensures a more uniform heat distribution, thus facilitating the maintenance of a stable temperature for the photovoltaic panels.

Figure 9 illustrates the existing lines and isotherms for a shunt chimney that incorporates an airflow **deflection** duct. In examining the streamlines, we observe the following: At low Reynolds number (Re=50), the air currents demonstrate a moderate degree of deflection through the shunt duct, thereby facilitating the modulation of airflow as required. As Re values increase, the deflection intensifies, thereby facilitating enhanced ventilation management and more effective heat extraction in regions with elevated temperatures. The utilization of isotherms facilitates an even distribution of heat, a consequence of optimized flow through the shunt duct. The configuration in question serves to mitigate the occurrence of hotspots and affords enhanced control of the temperature inside the chimney. Consequently, this solution is particularly well-suited to circumstances where thermal stability is of paramount importance.

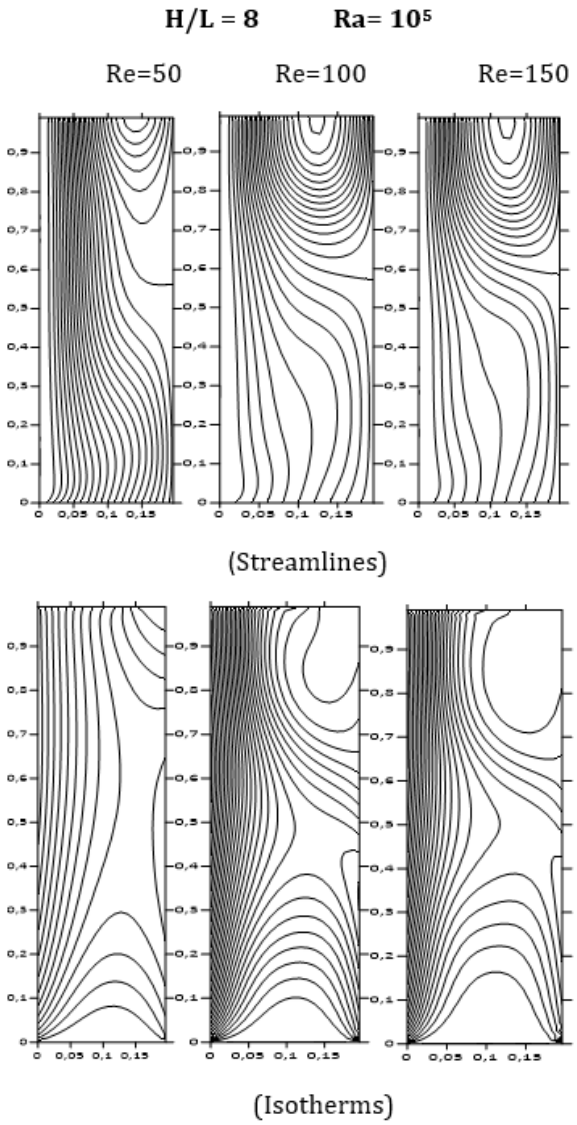

Figure 5: Streamlines and isotherms for simple chimneys

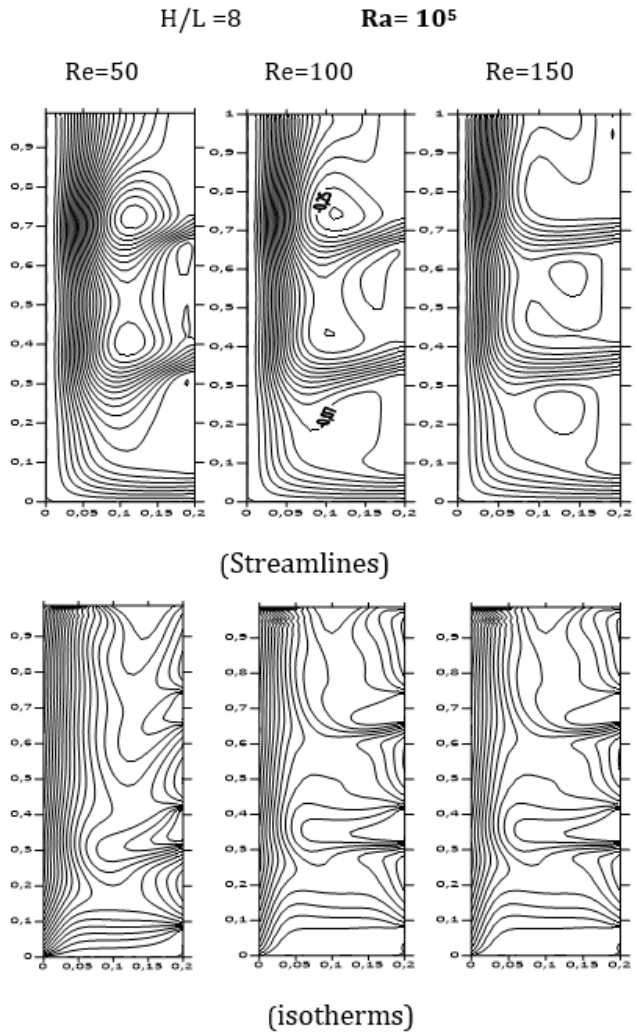

Figure 6: Streamlines and isotherms for the combined chimney

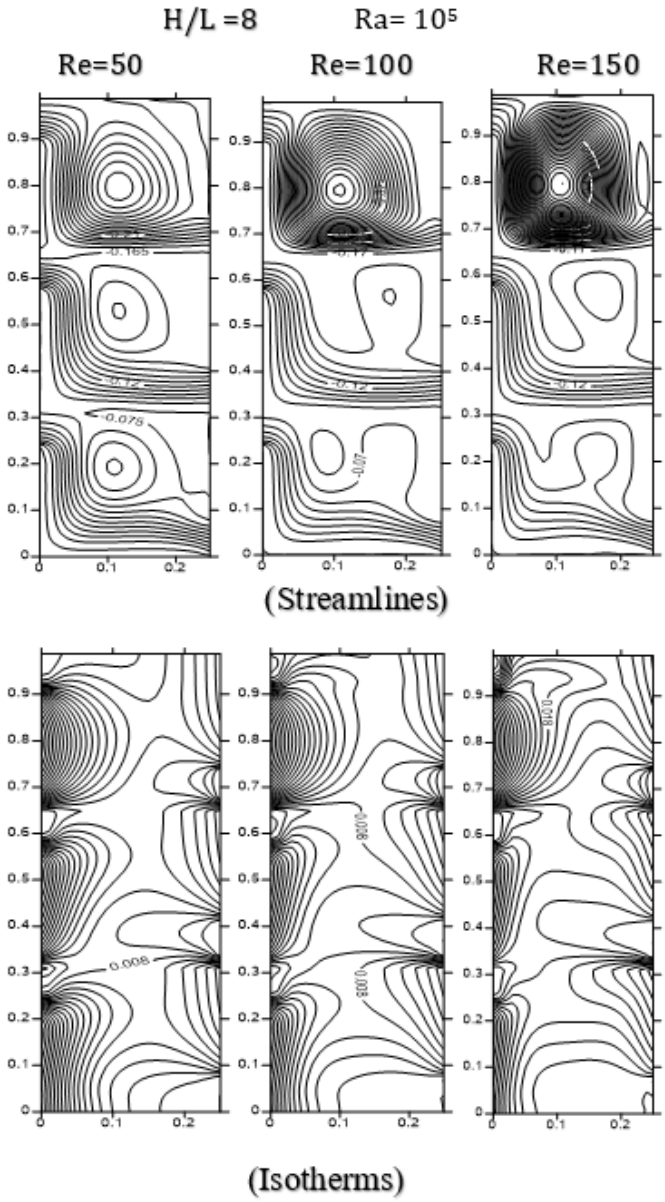

Figure 7: Streamlines and isotherms for the separated chimney

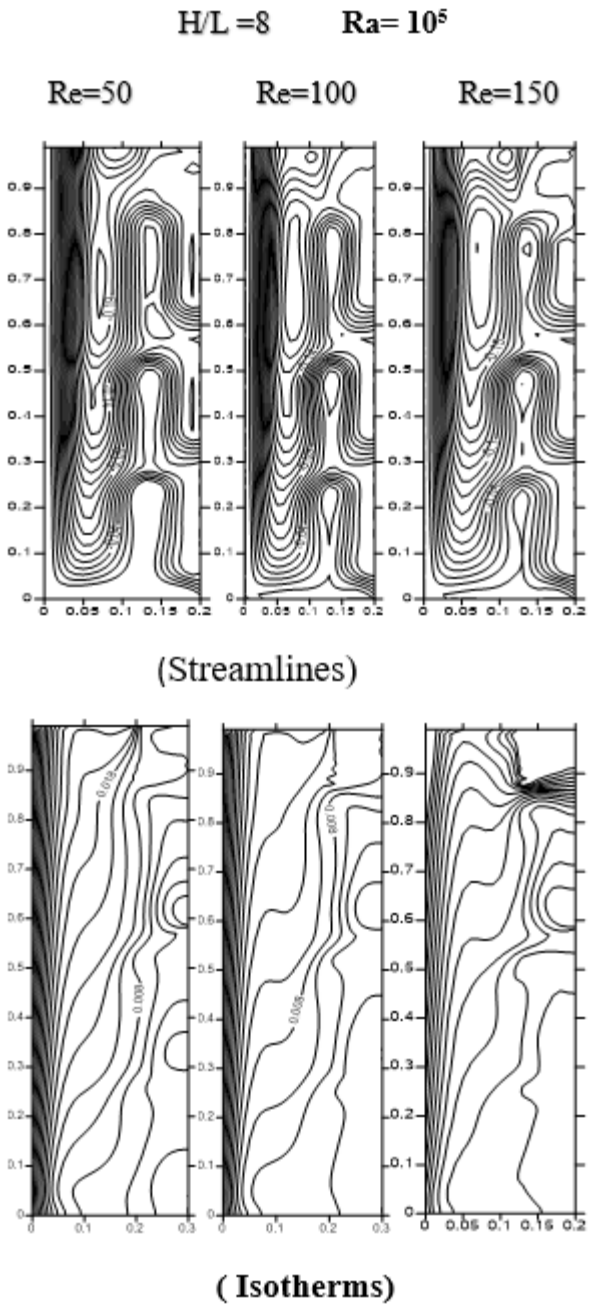

Figure 8: Streamlines and isotherms for the shunt chimney

3.3.2 Number of local Nusselt

The impact of Reynolds number (Re) on thermal performance is explored through the analysis of Figures 9 to 14. Figures 9, 10 and 11 show the variation in the local Nusselt number (Nu) for the separate stack at different Re levels. At low Re, Nu is relatively low, indicating limited heat transfer. However, at Re=150, Nu increases considerably, especially at the third level, indicating improved convection and heat dissipation due to flow segmentation. **Figure 12** illustrates a similar phenomenon for the combined stack, where increasing Re improves convection, resulting in higher Nu. This is due to the increased interaction between the air and the hot surfaces (absorbers). **Figure 13** shows the evolution of Nu in the simple stack, where the effect of Re is observable, but with lower Nu values compared with the other configurations. Finally, **Figure 14** shows the best performance for the shunt stack, where the increase in Re allows the flow to be concentrated in specific areas, maximising the Nu and improving the cooling of the PV panels. In summary, these figures show that increasing Re improves heat transfer, with optimum performance in both the combined and shunt configurations.

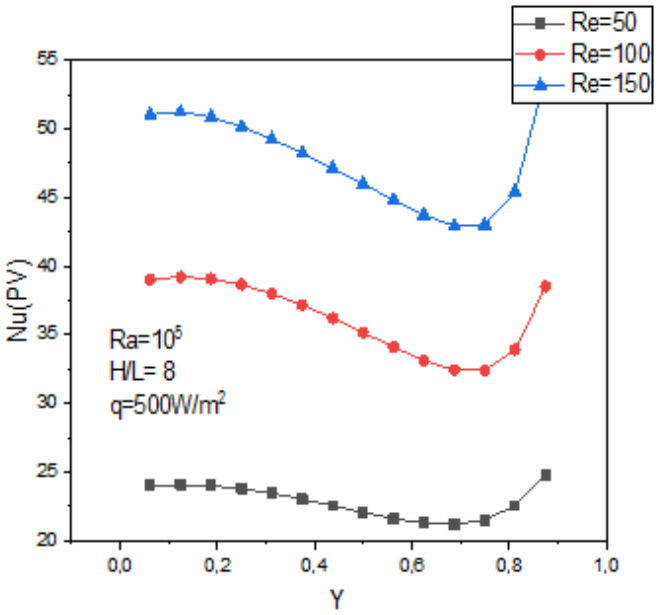

Figure 9: Variation of the local Nusselt number along the PVs of the separated chimney as a function of Reynolds (a- first level)

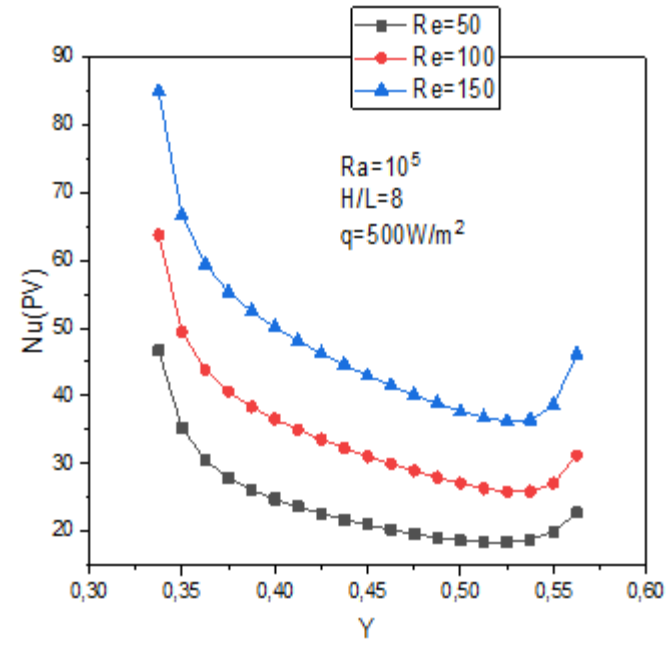

Figure 10: Variation of the local Nusselt number along the PVs of the separated chimney as a function of Reynolds (b-second level)

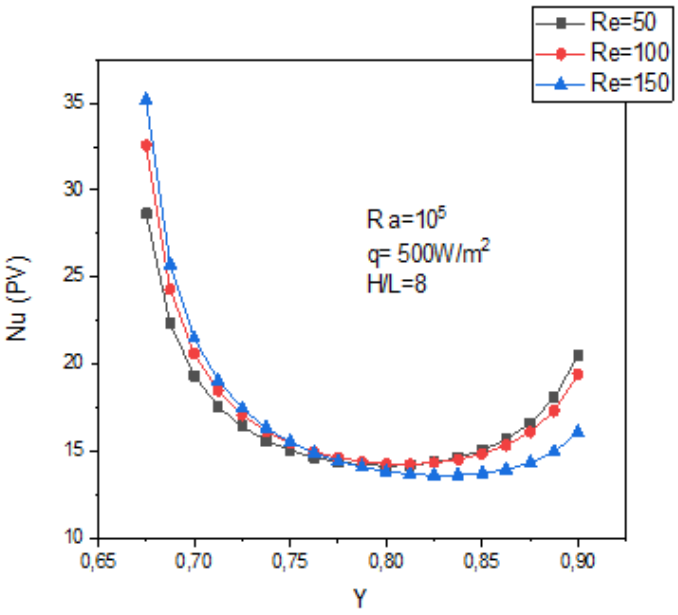

Figure 11: Variation of the local Nusselt number along the PVs of the separated chimney as a function of Reynolds c-third level)

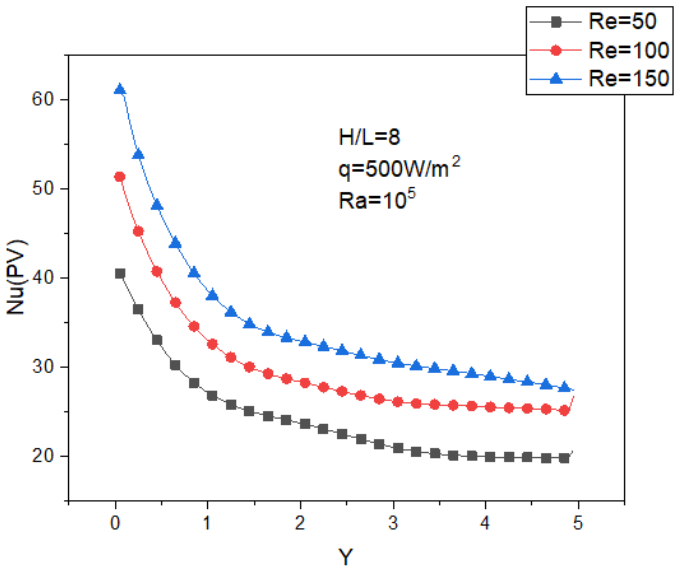

Figure 12: Variation of the local Nusselt number along the PVs of the combined chimney as a function of Reynolds

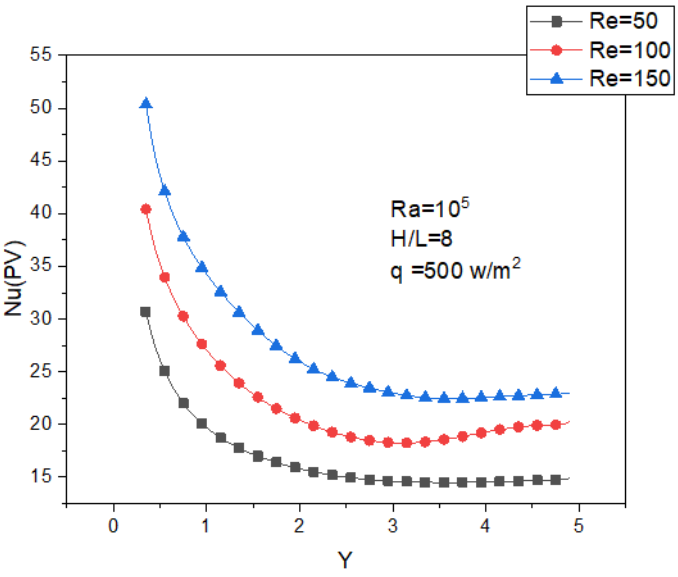

Figure13: Variation of the local Nusselt number along the PVs of the single chimney as a function of Reynolds

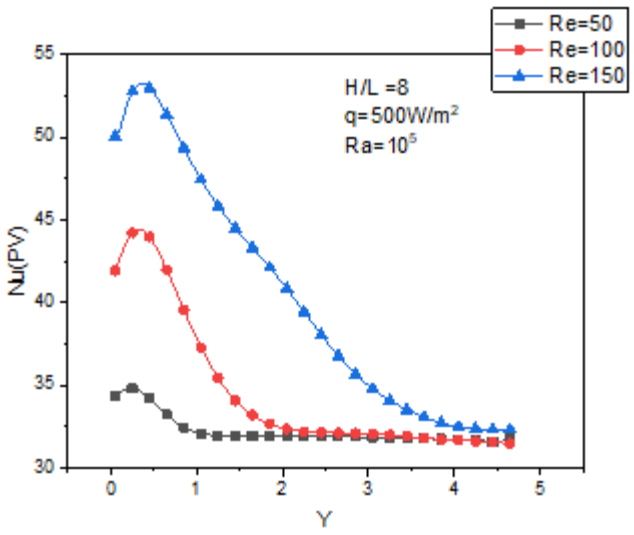

Figure 14: Variation of the local Nusselt number along the PVs of the shunt chimney as a function of Reynolds

3.3 Electrical and thermal performance of chimneys

Figures 15 to 19 compare the thermal and electrical performance of different stack configurations (simple, combined, separate and shunt) as a function of time and Reynolds number (Re). These performances include electrical efficiency, thermal efficiency, and air mass flow rate.

Figure 15 shows that the electrical efficiency of photovoltaic (PV) panels is strongly influenced by cell temperature, which in turn depends on the heat dissipation performance of each chimney. In the case of the simple chimney, the electrical efficiency decreases in the middle of the day, when temperatures reach their maximum. This loss of efficiency, which can be as much as 8%, results from insufficient heat dissipation. Thanks to a better interaction between the airflow and the heat absorbers, the combined chimney maintains a more stable electrical efficiency, with an increase of 5-8% compared with the simple chimney. The segmentation of the flow reduces hot spots, ensuring greater thermal stability. Electrical efficiency is improved by 4-7% compared with the simple chimney. Flexible flow management keeps panel temperatures at an optimum level. Electrical efficiency is maximised, with an increase of 6-10% compared with the simple configuration.

Figure 16 shows the thermal efficiency of chimneys as a function of time. Thermal efficiency remains low for the simple chimney (around 50-55%) due to the low natural convection capacity, which limits heat dissipation. With a thermal efficiency of 65-70%, the combined chimney benefits from the increased interaction between the absorbers and the airflow, especially in the middle of the day when thermal loads are high. Although slightly lower than the combined stack (60-65%), the separated stack ensures homogeneous and stable heat dissipation thanks to the segmentation. Thermal efficiency reaches 70-75%, thanks to the dynamic modulation of the airflow in the shunt stack, which is particularly effective in managing heat peaks in the middle of the day.

Figure 17 shows that thermal efficiency increases with Reynolds number (Re), reflecting more intense forced convection. The single stack remains limited, with an efficiency of less than 55% at Re=150. The combined stack reaches over 70%, thanks to better convection around the absorbers. The separate chimney offers stable efficiency at 65%, giving priority to thermal homogeneity. Finally, the shunt chimney achieves the best performance, with 75% Re=150, thanks to optimized flow management in critical areas.

Figure 18 shows that the electrical efficiency of PV panels increases with Re, thanks to better heat dissipation. The single stack is limited to 10% at Re=150, while the combined stack achieves 14% thanks to a significant reduction in panel temperature. The separated chimney offers 13% efficiency with homogeneous dissipation, and the shunt chimney, the highest-performing chimney, achieves 15% by optimizing flow management for efficient cooling.

Figure 19 shows that the mass flow rate is directly related to Re and plays a key role in thermal performance. In the simple chimney, the flow rate increases with Re, but remains limited by its design. The combined chimney, with optimized absorbers, promotes a higher flow rate, improving thermal and electrical efficiency. The separated stack distributes mass flow evenly between its segments, ensuring balanced heat dissipation. Finally, the shunt stack maximises mass flow

by concentrating the flow in critical areas, optimising overall performance

The findings of this study demonstrated that the configuration of the combined chimney with multiple air inlets enhances convective heat transfer. This leads to an enhancement in the Nusselt number, notably at elevated Reynolds numbers. This observation aligns with the findings of Sopian et al. [25], who demonstrated that double-pass PV/T air collectors facilitate enhanced heat transfer through optimized air circulation. Our study, however, is a more comprehensive one, incorporating multiple inlet ventilation, which has the additional effect of increasing heat dissipation and reducing the temperature of the PV cells. In contrast, the separated chimney is distinguished by its capacity to segment the airflow, which facilitates the uniform distribution of heat across the ventilation channel. This approach bears resemblance to the findings of Hegazy [26], who investigated the impact of diverse flow channels in PV/T collectors. These conclusions indicated that segmentation of the flow enhances thermal conductivity. Notwithstanding the foregoing, our distinct stack configuration exhibits superior results in terms of thermal stability, which may be pivotal for applications necessitating precise temperature control in multi-story edifices. The stability of the electrical efficiency observed for the combined and shunt configurations in this study is corroborated by the findings of Chen et al [21], who demonstrated that an air-cooled PV/T system with forced circulation improves the electrical efficiency by reducing the temperature of the PV cells. Moreover, the research conducted by Nagano et al. [22] demonstrated that a PV/T system equipped with a glass cover exhibited enhanced thermal efficiency, yet concurrently exhibited a decline in electrical efficiency due to condensation and an internal temperature rise. In comparison, the shunt stack configuration, which diverts a portion of the airflow, permits the implementation of more efficacious ventilation while circumventing the issue of condensation. This configuration also ensures that the optimal temperature for the photovoltaic cells is maintained. This demonstrates that designs incorporating multiple air inlets and outlets demonstrate superior temperature management capabilities in comparison to the covered systems studied by Nagano et al.[22] and Lare et al[27]

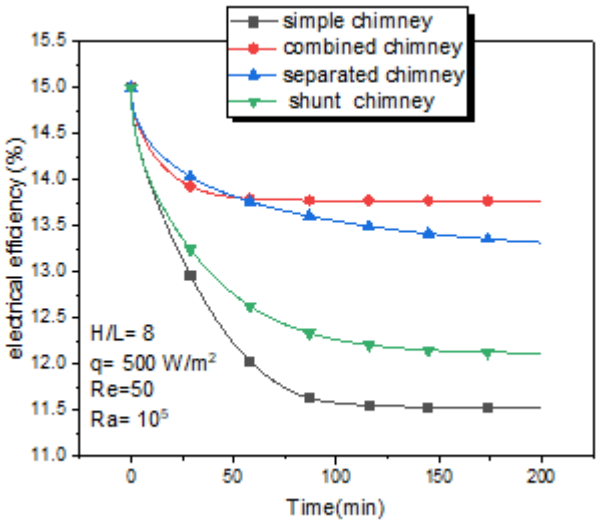

Figure15: Variation in electrical efficiency as a function of time

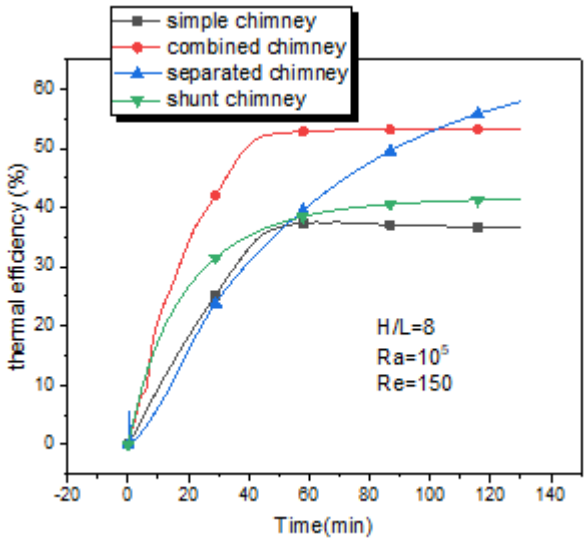

Figure16: Variation in thermal efficiency as a function of time

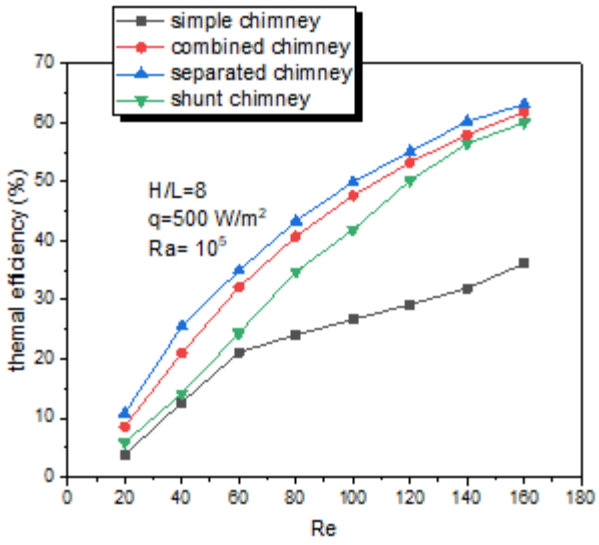

Figure 17: Variation in thermal efficiency as a function of Reynolds number

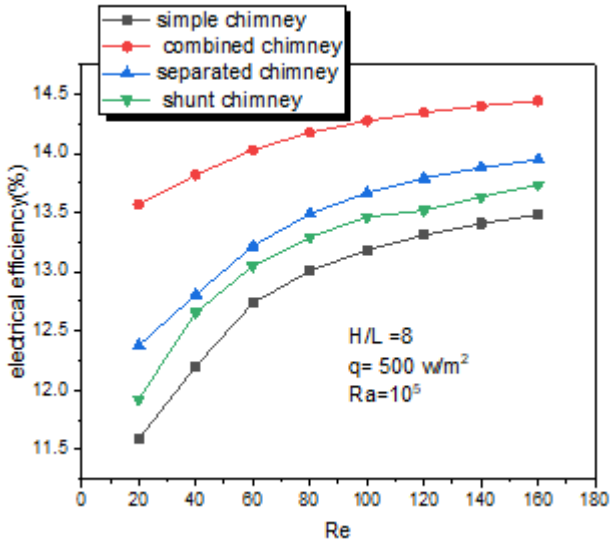

Figure 18: Variation in electrical efficiency as a function of Reynolds number

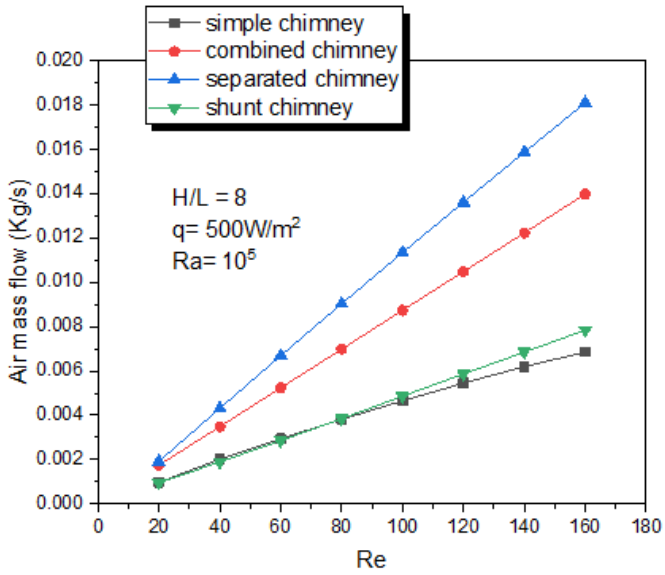

Figure 19: Variation in mass flow rate as a function of Reynolds number

4. Conclusion

This research study illuminates the enhanced functionality of photovoltaic/thermal (PV/T) hybrid solar chimneys integrated into multi-story edifices, with a particular focus on the incorporation of multiple air inlets. The findings demonstrate that the combined, separated, and shunt chimney configurations facilitate superior heat dissipation and enhanced electrical output stability in comparison to single-entry systems. Notably, the separated stack, due to the segmentation of the airflow, ensures uniform heat distribution, reducing the likelihood of overheating and increasing the conversion efficiency of the photovoltaic cells. These findings indicate that PV/T systems with such configurations could be utilized for passive cooling applications in multi-story buildings, thereby optimizing energy production while reducing air conditioning requirements. In practical terms, these systems could be particularly well-suited to residential or administrative buildings in hot regions, where effective heat management is essential for maintaining thermal comfort and reducing energy consumption. Moreover, the incorporation of solar chimneys with enhanced ventilation systems may facilitate the creation of more sustainable buildings, reducing energy costs whilst optimizing the utilization of available solar energy. These solutions are part of an eco-responsible construction and energy transition perspective, offering a promising avenue for reducing the carbon footprint of buildings while optimally utilizing renewable energy.

Nomenclature

Letters

c_p :	Calorific capacity (J. Kg^{-1}. $°C^{-1}$)
d:	Chimney width (m)
g:	Acceleration of gravity ($m.s^{-2}$)
h:	Convective Transfer Coefficient ($W\ m^{-2}K^{-1}$)
H:	Overall height of the chimney(m)
D:	The ratio of total height to the width of the chimney
S:	The ratio of the height of the second level to the width of the chimney
A:	The ratio of the height of the first level to the width of the chimney
T:	The ratio of the first entrance to the width of the chimney
K:	The ratio of the height of the third level to the width of the chimney
P :	The ratio of the height of the second level to the width of the chimney
L:	Total length of the room (m)
Gr:	Grashof number (-)
Pr:	Prandtl number (-)
Re:	Reynolds number (-)
t:	Time (s)
T:	Temperature (K)
T_a:	Ambient air temperature (K)
u, v :	Components of directional velocity x et y ($m.s^{-1}$)
U, V :	Dimensionless components of speed in directions X et Y, $U = u/u_0$, $V = v/u_0$, (-)
U_0:	Air inlet velocity in the chimney ($m.s^{-1}$)
X, Y:	Dimensionless Cartesian coordinates (-)
x, y :	Cartesian coordinates (m)

Greek Letters

Ω:	Dimensionless vorticity(-)
ω:	Dimensional vorticity (s^{-1})
ψ:	Dimensional Current Function ($m^2.s^{-1}$)
Ψ:	Dimensionless current function (-)
Θ:	Dimensionless Temperature (-)
τ:	Dimensionless Time(-)
λ:	Coefficient of Thermal Conductivity ($W.m^{-1}.°C^{-1}$)
μ:	Dynamic Viscosity of Air ($Kg.m^{-1}.s^{-1}$)
ρ:	Air density ($Kg.m^{-3}$)
τ :	Transmission coefficient
η_{el}:	Electrical efficiency of cells PV(-)
η_{th} :	Thermal efficiency of the chimney (-)
Dm :	mass flow rate (Kg/s)
Φ:	The density of solar flux ($W.m^{-2}$)

References

[1] Z. Kang, Z. Lu, G. Song, and Q. Yao, "A numerical study of dual-inlet air-cooled PV/T solar collectors with various airflow channel configurations," *Sustainability,* vol.14,no.16, p.9897,2022.https://doi.org/10.3390/su14169897

[2] T. Nualboonrueng, P. Tuenpusa, Y. Ueda, and A. Akisawa, "Field experiments of PV-thermal collectors for residential application in Bangkok," *Energies,* vol. 5,no.4,pp.1229-1244,2012. https://doi.org/10.3390/en5041229

[3] S. N. Jahromi, A. Vadiee, and M. Yaghoubi, "Exergy and economic evaluation of a commercially available PV/T collector for different climates in Iran," *Energy Procedia,* vol. 75, pp. 444-456, 2015. https://doi.org/10.1016/j.egypro.2015.07.416

[4] M. Rosa-Clot, P. Rosa-Clot, G. Tina, and C. Ventura, "Experimental photovoltaic-thermal Power Plants based on TESPI panel," *Solar Energy,* vol. 133, pp. 305-314, 2016. https://doi.org/10.1016/j.solener.2016.03.024

[5] M. E. H. Attia, M. E. Zayed, A. Kabeel, A. Khelifa, K. Irshad, and S. Rehman, "Numerical analysis and design of a novel solar photovoltaic thermal system using finned cooling channel structures embedded with air/TiO2–water nano bi-fluid," *Solar Energy,* vol. 269, p. 112368, 2024. https://doi.org/10.1016/j.solener.2024.112368

[6] M. E. A. Slimani, M. Amirat, I. Kurucz, S. Bahria, A. Hamidat, and W. B. Chaouch, "A detailed thermal-electrical model of three photovoltaic/thermal (PV/T) hybrid air collectors and photovoltaic (PV) module: Comparative study under Algiers climatic conditions," *Energy conversion and management,* vol. 133, pp. 458-476,2017. https://doi.org/10.1016/j.enconman.2016.10.066

[7] M. Patil, A. Sidramappa, S. K. Shetty, and A. M. Hebbale, "Experimental study of solar PV/T panel to increase the energy conversion efficiency by air cooling," *Materials Today: Proceedings,* vol. 92, pp. 309-313, 2023. https://doi.org/10.1016/j.matpr.2023.05.007

[8] J. Tonui and Y. Tripanagnostopoulos, "Performance improvement of PV/T solar collectors with natural air flow operation," *Solar energy,* vol. 82, no. 1,pp.1-

12,2008. https://doi.org/10.1016/j.solener.2007.06.004
[9] H.-U. Choi and K.-H. Choi, "Performance evaluation of PV/T air collector having a single-pass double-flow air channel and non-uniform cross-section transverse rib," *Energies,*vol.13,no.9,p.2203,2020. https://doi.org/10.3390/en13092203
[10] N. Badi and A. H. Laatar, "Improved cooling of photovoltaic panels by natural convection flow in a channel with adiabatic extensions," *Plos one,* vol. 19, no. 7,p.e0302326,2024. https://doi.org/10.1371/journal.pone.0302326
[11] N. Boulfaf, J. Chaoufi, A. Ghafiri, and A. Elorf, "Thermal study of hybrid photovoltaic thermal (PV-T) solar air collector using finite element method," *International Journal of Renewable Energy Research,* vol. 6, no. 1, pp. 171-182, 2016.
[12] W. Yu, Y. Lei, G. Wang, W. Chan, T. Wang, and Y. Tian, "Simulation and optimization on a novel air-cooled photovoltaic/thermal collector based on micro heat pipe arrays," *Applied Thermal Engineering,* vol. 255, p. 123986,2024. https://doi.org/10.1016/j.applthermaleng.2024.123986
[13] S. Zine, B. Djedjiga, S. Fethya, L. Salah, and B. Ahmed, "Experimental Study of Hybrid Photovoltaic (PV/T) Thermal Solar Collector with Air Cooling for Domestic Use: A Thermal and Electrical Performances Evaluation," *Journal of Advanced Research in Fluid Mechanics and Thermal Sciences,* vol. 116, no. 1,pp.170-183,2024. https://doi.org/10.37934/arfmts.116.1.170183
[14] A. Shahsavar and M. Ameri, "Experimental investigation and modeling of a direct-coupled PV/T air collector," *Solar Energy,* vol. 84, no. 11,pp.1938-1958,2010. https://doi.org/10.1016/j.solener.2010.07.010
[15] N. Van Hap, M. T. Dam, N. H. Khoi, and N. M. Phu, "Parametric Investigation and Optimization of the Photovoltaic-Thermal Air Heater," *Journal of Advanced Research in Fluid Mechanics and Thermal Sciences,* vol. 120,no.2,pp.67-81,2024. https://doi.org/10.37934/arfmts.120.2.6781
[16] Y. B. Assoa and C. Ménézo, "Dynamic study of a new concept of photovoltaic–thermal hybrid collector," *Solar Energy,* vol. 107, pp. 637-652, 2014, doi: 10.1016/j.solener.2014.05.035. https://doi.org/10.1016/j.solener.2014.05.035
[17] K. Sahlaoui, H. Oueslati, and S. B. Mabrouk, "Thermal and electrical performance evaluation of hybrid air PV/T collector–numerical analysis and experimental study," *International Journal of Sustainable Energy,* vol. 40, no. 9, pp. 889-909,2021. https://doi.org/10.1080/14786451.2021.1884076
[18] J. Clarke, J. Hand, C. Johnstone, N. Kelly, and P. Strachan, "Photovoltaic-integrated building facades," *Renewable energy,* vol. 8, no. 1-4, pp. 475-479, 1996. https://doi.org/10.1016/0960-1481(96)88902-6
[19] B. Agrawal and G. Tiwari, "Optimizing the energy and exergy of building integrated photovoltaic thermal (BIPVT) systems under cold climatic conditions," *Applied energy,*vol.87,no.2,pp.417-426,2010. https://doi.org/10.1016/j.apenergy.2009.06.011
[20] J. Ji, C. Luo, T.-T. Chow, W. Sun, and W. He, "Thermal characteristics of a building-integrated dual-function solar collector in water heating mode with natural circulation," *Energy,* vol. 36, no. 1, pp. 566-574, 2011. https://doi.org/10.1016/j.energy.2010.10.004
[21] Y. Chen, A. Athienitis, and K. Galal, "Modeling, design and thermal performance of a BIPV/T system thermally coupled with a ventilated concrete slab in a low energy solar house: Part 1, BIPV/T system and house energy concept," *Solar energy,* vol. 84, no. 11, pp. 1892-1907,2010. https://doi.org/10.1016/j.solener.2010.06.013
[22] K. Nagano, T. Mochida, K. Shimakura, K. Murashita, and S. Takeda, "Development of thermal-photovoltaic hybrid exterior wallboards incorporating PV cells in and their winter performances," *Solar Energy Materials and Solar Cells,* vol. 77, no. 3, pp. 265-282, 2003.https://doi.org/10.1016/S0927-0248(02)00348-3
[23] S. Pantic, L. Candanedo, and A. Athienitis, "Modeling of energy performance of a house with three configurations of building-integrated photovoltaic/thermal systems," *Energy and buildings,* vol. 42, no. 10, pp. 1779-1789, 2010. https://doi.org/10.1016/j.enbuild.2010.05.014
[24] A. M. S. BOUABDALLAH, A. BENCHATTI & A. HAMINI, "<convection-mixte-dans-une-cavité-carrée-contenant-des-portes-d'entrée-et-de-sortie-d'air.pdf>," *Revue des sciences et sciences de l'ingénieur,* vol. 01, pp. 1-9, 2011.
[25] K. Sopian, K. Yigit, H. Liu, S. Kakac, and T. Veziroglu, "Performance analysis of photovoltaic thermal air heaters," *Energy Conversion and management,* vol.

37, no. 11, pp.1657-1670,1996. https://doi.org/10.1016/0196-8904(96)00010-6

[26] A. A. Hegazy, "Comparative study of the performances of four photovoltaic/thermal solar air collectors," *Energy Conversion and management,* vol. 41, no. 8, pp. 861-881, 2000. https://doi.org/10.1016/S0196-8904(99)00136-3

[27] D. Y. Lare, Y. Nougblega, K. Kpode, and K. A. Amou, "Enhancing Thermoelectric Efficiency Through Combined and Shunt Solar Chimneys: An Investigation of Vented Photovoltaic Panels with Multiple Inlets," *International Journal of Heat and Technology,* vol. 42, no. 5,pp.1709-1720,2024, https://doi.org/10.18280/ijht.420525